Ultraviolet optical and microstructural properties of MgF_2 and LaF_3 coatings deposited by ion-beam sputtering and boat and electron-beam evaporation

Detlev Ristau, Stefan Günster, Salvador Bosch, Angela Duparré, Enrico Masetti, Josep Ferré-Borrull, George Kiriakidis, Francesca Peiró, Etienne Quesnel, and Alexander Tikhonravov

Single layers of MgF_2 and LaF_3 were deposited upon superpolished fused-silica and CaF_2 substrates by ion-beam sputtering (IBS) as well as by boat and electron beam (e-beam) evaporation and were characterized by a variety of complementary analytical techniques. Besides undergoing photometric and ellipsometric inspection, the samples were investigated at 193 and 633 nm by an optical scatter measurement facility. The structural properties were assessed with atomic-force microscopy, x-ray diffraction, TEM techniques that involved conventional thinning methods for the layers. For measurement of mechanical stress in the coatings, special silicon substrates were coated and analyzed. The dispersion behavior of both deposition materials, which was determined on the basis of various independent photometric measurements and data reduction techniques, is in good agreement with that published in the literature and with the bulk properties of the materials. The refractive indices of the MgF_2 coatings ranged from 1.415 to 1.440 for the wavelength of the ArF excimer laser (193 nm) and from 1.435 to 1.465 for the wavelength of the F_2 excimer laser (157 nm). For single layers of LaF_3 the refractive indices extended from 1.67 to 1.70 at 193 nm to ~1.80 at 157 nm. The IBS process achieves the best homogeneity and the lowest surface roughness values (close to 1 nm_{rms}) of the processes compared in the joint experiment. In contrast to MgF_2 boat and e-beam evaporated coatings, which exhibit tensile mechanical stress ranging from 300 to 400 MPa, IBS coatings exhibit high compressive stress of as much as 910 MPa. A similar tendency was found for coating stress in LaF_3 single layers. Experimental results are discussed with respect to the microstructural and compositional properties as well as to the surface topography of the coatings.

OCIS codes: 310.3840, 310.6860, 310.6870.

1. Introduction

In the course of the rapid growth of applications for deep ultraviolet–vacuum ultraviolet (DUV–VUV) lasers in many future-oriented fields, an increasing demand for optical components with low optical losses, high stability, and long lifetimes has emerged in optical technology.[1] In particular, the extremely demanding road map in semiconductor lithography that aims toward achieving a spatial resolution significantly below 100 nm in chip fabrication as well as micromaterial processing with excimer lasers imposes new challenges for the production of optical components that surpass the current capabilities of present production processes. The economic efficiency of these modern applications is directly dependent on the quality of the dielectric coatings deposited upon the optical components used in the beam lines and the laser systems. Therefore the achievement

D. Ristau (dr@lzh.de) and S. Günster are with Laser Zentrum Hannover, 30419 Hannover, Germany. S. Bosch, J. Ferré-Borrull, and F. Peiró are with the Laboratori d'Optica i Departamento Electrònica, Universitat de Barcelona, E-08028 Barcelona, Spain. A. Duparré is with the Fraunhofer Institut für Angewandte Optik und Feinmechanik, D-07745 Jena, Germany. E. Masetti is with the Ente per le Nuove Technologie, l'Energia e l'Ambiente, 00060 Rome, Italy. G. Kiriakidis is with the Materials Group, Foundation for Research and Technology—Hellas, 71110 Heraklion Crete, Greece. Etienne Quesnel is with the Laboratoire d'Electronique de Technologie et d'Instrumentation, 38054 Grenoble, Cedex 9, France. A. Tikhonravov is with the Research Computer Center, Moscow State University, Moscow 119899, Russia.

Received 25 September 2001; revised manuscript received 24 January 2002.

0003-6935/02/163196-09$15.00/0

Table 1. Deposition Parameters of MgF_2 and LaF_3 Layers[a]

Material/Process	Process Type	T_s (°C)	Deposition Rate (nm/s)	Pumping System	Base Pressure (Pa)
MgF_2/IBS	Reactive IBS, rf source	maximum 60	0.04	Cryopump	Reactive, 5×10^{-6}
MgF_2/PVD1	Thermal e-beam	300	0.70	Cryopump	6×10^{-4}
MgF_2/PVD2	Thermal Mb boat	300	0.80	Diffusion pump, LN_2 trap	7×10^{-4}
LaF_3/IBS	Reactive IBS rf source	maximum 60	0.04	Cryopump	Reactive, 5×10^{-6}
LaF_3/PVD1	Thermal Mb boat	300	0.30	Cryopump	1×10^{-3}
LaF_3/PVD2	Thermal Mb boat	350	0.40	Diffusion pump, LN_2 trap	5×10^{-4}

[a]Parameters for the deposition of the MgF_2 and LaF_3 layers investigated. Deposition rate in units of geometric thickness per second; T_s substrate temperature.

of adapted optical coatings is considered one of the major goals for success of industrial DUV–VUV laser applications, and, as a consequence, current thin-film research is concentrated on the improvement of advanced coating processes.[2–4] For the spectral range 150–250 nm, MgF_2–LaF_3 is considered a material combination that is likely to be a highly desirable component of optical coating systems with low losses and high thresholds to laser-induced damage.[5–7] The present fundamental study of MgF_2 and LaF_3 single layers was performed within the framework of the European Training and Mobility of Researchers network, New Optimization Concepts for High Quality UV-Coatings,[8] by a consortium of thin-film laboratories in Europe. Within joint experiments single layers of these materials were produced by selected processes with optimized deposition parameters and characterized in terms of their optical and structural properties. In what follows, various deposition methods used for the fluoride materials and the characterization techniques employed are described. The measurement results are discussed in the context of the deposition parameters and in consideration of the intended applications for the coatings.

2. Experiment

A. Deposition of MgF_2 and LaF_3 Single Layers

Coatings were deposited upon selected superpolished UV-grade quartz and calcium fluoride substrates that had been purchased from several vendors and characterized in the preparation phase of the joint experiments. Besides substrates of high optical quality for the DUV–VUV spectral range, silicon substrates specially adapted for stress measurements and for use in investigations of film structure were also coated in each run. The target thickness of all single layers was 6 quarter-wave optical thickness at 193 nm. The coatings were produced by three laboratories within the consortium; each laboratory used its specific coating method.

The parameters of the three deposition processes employed for production of the single-layer coatings are summarized in Table 1. In ion-beam sputtering (IBS),[9,10] the single layers were deposited from pure hot-pressed targets in a reactive atmosphere of diluted fluorine. A commercial Nordiko radio-frequency ion source, a beam neutralizer, and xenon sputtering gas were used for the IBS deposition. During deposition the substrate holder rotated and was not heated, so the substrate temperature remained below 60 °C. All samples of each deposition material were deposited in the same batch, at a typical sputtering rate of 0.04 nm/s. Preceding 25-nm thick sputtered alumina films were deposited upon the silicon substrates to improve the adhesion of the subsequent MgF_2 layers.

The e-beam process, which was applied only for the MgF_2 layers, was performed in a specially adapted commercial deposition system (Balzers BAK 640). Before the deposition the system was pumped down to a base pressure of less than 6×10^{-4} Pa by a cryopump arrangement. The MgF_2 coatings were deposited at a typical deposition rate of 0.7 nm/s at a substrate temperature of 300 °C. For the deposition of LaF_3 coatings, a boat evaporation process was installed in the same plant. In that case the deposition rate was reduced to 0.3 nm/s and the substrate temperature was adjusted to 300 °C. The third coating laboratory within the network employed a boat evaporation process for MgF_2 coatings that was operated with a deposition rate of approximately 0.8 nm/s and a substrate temperature of 300 °C. The coating process was started at a base pressure of 7×10^{-4} Pa in a Balzers BAK 600 deposition chamber that was equipped with a conventional diffusion pumping system. With the exception of a substrate temperature of 350 °C, a base pressure of 5×10^{-4} Pa, and a rate of 0.4 nm/s, similar conditions were chosen for the LaF_3 coatings.

B. Thin-Film Characterization

For determination of the refractive indices and the extinction coefficients, several commercial facilities and a self-constructed spectrophotometric setup were employed in conjunction with a variety of software tools.[11–13] Besides commercial software environments,[11] several data-reduction techniques including Cauchy- and Sellmeier-type dependencies were used to calculate the dispersion curves for the wavelength range 130–1200 nm. Before the characterization of the single-layer samples, selected reference sub-

strates were carefully characterized in terms of refractive-index data and substrate absorption in the VUV spectral range. The absorption of the substrates became apparent below 200 nm, but analytical modeling is not precise in this spectral region. One can develop a useful procedure for determining the extinction coefficient by fitting the T spectra of the bare substrate and assuming single-pass losses. The contribution of the back sides of the superpolished substrates (surface roughness below 0.2 nm) was taken into account in the spectrometric analysis, which concentrated on measurements at near-normal incidence.

Data reduction in the VUV spectral range has to compete with the strongly increasing absorption of the substrate and the deposition material. For this wavelength region of 130–200 nm we determined the refractive index with a data-reduction method that used the transmittance and reflectance data in this absorptive region as well as the experimental data in the absorption-free range. Film thickness values were deduced from the interference pattern in the absorption-free region, and the dispersion was described by the first-order Sellmeier equation for the whole spectral range. Finally, absorption was calculated directly from the transmittance and reflectance data; substrate absorption, which was determined from uncoated retained samples, was taken into account. The complete process was repeated in an iterative procedure to minimize the figure of merit. Various models for the inhomogeneity of the layers were considered in the fitting process. Because, for all single layers, total scattering levels that ranged below the precision of the spectrophotometers employed were measured at 193 nm, scattering effects were neglected in the analysis. To increase the accuracy of refractive-index determination it will be desirable to develop new mathematical algorithms that will allow scattering and absorption losses to be separated and the parameters that characterize these losses to be determined along with the refractive index.

For measurement of the stress in the thin films, the coatings were deposited upon (111) oriented single-crystal silicon substrates (50 mm $\times$ 5 mm, 1 mm thick). The residual internal stress (σ) in the films was determined from the difference in the radii of curvature of the substrates before and after deposition of the coating by use of a Fizeau interferometer.[14]

Total backscattering (TBS) of the components was measured at 633 and 193 nm with a setup described in detail elsewhere.[15,16] The setup included a Coblentz sphere collecting the backscattered radiation over an angular range of 2°–85°, several sources in the spectral region from 193 to 10.6 μm, a detection unit, and a sample positioning system. For the samples under study the equipment was adjusted to near-normal incidence of the test beam on the sample surface. The scatter values were recorded on each sample in two one-dimensional scans that were perpendicular to each other. The spot size of the laser beam was 0.4 mm at 633 nm and 4 mm at 193 nm. A Digital Instruments Dimension 3000 atomic-force microscope (AFM) was operated in the tapping mode for direct imaging of the surface features and for roughness determination. For each sample, scan areas of 1-, 10-, and 50-μm edge length were evaluated. Power spectral densities were calculated to yield the rms roughness that was relevant for an extended spatial frequency range.[17] The crystalline structure was assessed by x-ray diffraction that used the grazing incidence of a CuK_α line in a Siemens D500 diffractometer. To determine layer composition we obtained depth profiles by using x-ray photoelectron spectroscopy from the monochromatic AlK_α line and Ar^+ low-energy (3-kV) sputtering with a Phi 5500 instrument.

For transmission electron microscopy of layers grown upon silicon substrates, plane-view specimens were prepared by conventional mechanical grinding and dimpling up to 30 μm, followed by a final Ar^+-ion bombardment at a low angle of incidence at 3 kV. Samples for cross-section observations were prepared with the same procedure on previously cleaved and face-to-face-glued samples. Observations were carried out with Hitachi H-800 NA and Philips CM30 electron microscopes working at 200 and 300 kV, respectively. Low-dose observation conditions were used to avoid degradation of the fluoride layers under *e*-beam illumination.

3. Results

The joint experiment was designed in three steps for each material. The first step comprised the preparation of the substrates and the coatings as well as an initial spectrophotometric inspection at the coating laboratories. In the second step the samples were collected by one of the laboratories in the consortium for nondestructive investigation of the surface properties by AFM and TBS measurements. The final step was started after a preliminary assessment of the data was available and included the distribution of the sample set among the consortium partners for microscopic studies of the structural properties and the composition of the films. Retained samples of each material treated by each process were stored for further investigations of the absorption behavior and of the laser-induced damage thresholds of the materials. In the following subsections, selected results of the characterization activities are illustrated, compared, and discussed.

A. Index of Refraction

For calculation of the dispersion behavior from spectrophotometric scans, three different algorithms were employed and compared for each sample. Most dispersion curves calculated by the different analytical approaches indicated good agreement within a margin of error of approximately 1%. The major sources of error could be attributed to experimental problems, especially to differences in the normalization of transmittance and reflectance data. By utilizing the OptiRE program[11] we found that all the MgF_2 films were generally homogeneous; meanwhile,

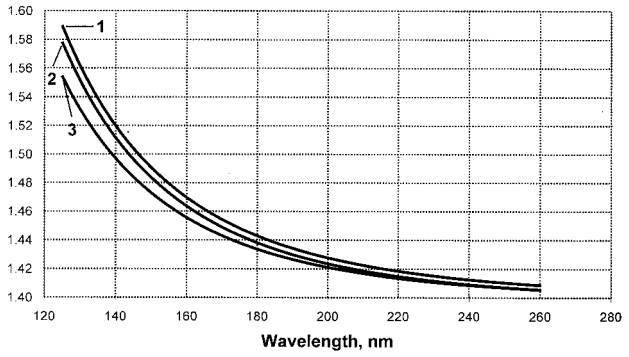

Fig. 1. Dispersion curves of MgF_2 films deposited by the PVD2 upon CaF_2 substrates. Curves represent refractive index relative to wavelength of samples coated in one batch upon selected positions within the substrate holder. A linear inhomogeneity of −2.5% was assumed for the calculation with best match to the experimental data.

a slight inhomogeneity of approximately −2.5% was observed for some boat and e-beam evaporation (PVD) LaF_3 samples. Figure 1 presents typical wavelength dependencies of the refractive index for different MgF_2 films deposited by the MgF_2 PVD2 process upon CaF_2 substrates for the wavelength range 130–260 nm. In Fig. 2 the dispersion behavior of process PVD2 for LaF_3 is illustrated for the DUV–VUV spectral region. In the DUV/VUV spectral region the data-reduction procedures are severely influenced by absorption, scattering, and also contamination effects in the layers as well as by higher margins of error that may appear during the spectrophotometric measurements in the VUV spectrophotometric systems. Therefore, to study the effects of the individual deposition conditions on the optical properties of the coatings in detail we performed extended calculations for a wavelength range above 200 nm on the basis of the available algorithms.[12,18] In summary, the dispersion behavior of both deposition materials is in good agreement with the values published in the literature[19,20] and with the bulk properties of the materials.

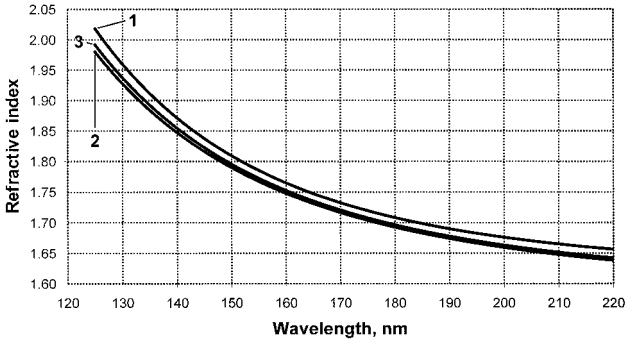

Fig. 2. Dispersion curves of LaF_3 films deposited by PVD2 upon CaF_2 substrates. The curves represent samples coated in one batch onto selected positions within the substrate holder.

B. Coating Stress

The coating stress data for the single layers are compiled in Table 2 relative to the substrate temperatures employed in the various processes. Independently of the material, the residual stresses are tensile for both of the evaporation processes and compressive for the IBS process. For these materials and coating processes, chiefly intrinsic contributions to the total mechanical stress have to be considered. The intrinsic component is influenced by the microstructural properties and the thermal properties of the coatings. For the PVD layers, which tend to a columnar growth, intrinsic stress effects can be described mainly by the difference in the thermal expansion coefficients of the layer material and the silicon substrate. For example, a calculation results in an estimation of approximately 350 MPa for the tensile thermal stress in MgF_2 layers, which is close to the measured values. Considering the thermal expansion coefficient (1.4×10^{-5} K^{-1}) of bulk LaF_3, which is in the same range as the expansion coefficient of MgF_2 and is nearly independent of the crystal orientation, the intrinsic stress in LaF_3 PVD layers is significantly lower than expected. The small compressive component may be attributed to structural effects in LaF_3. In contrast to those in PVD coatings, stress effects in the IBS films are dominated by the special microstructure produced in this energetic process. In IBS the admolecules that carry a high kinetic energy, in the range of several electron volts impinge upon the growing layer, which results in the formation of a dense film structure. In some cases this structure has an even higher packing density than the corresponding bulk material, leading to high compressive stress in the layers.

C. Total Backscattering and Surface Roughness

TBS values of the MgF_2 and LaF_3 single coatings upon several substrates are listed in Table 3 for wavelengths 633 and 193 nm, respectively. Each of the values in Table 3 results from averaging the total

Table 2. Deposition Temperature and Coating Stress[a]

Process	Material/Process					
	MgF_2/IBS	MgF_2/PVD1	MgF_2/PVD2	LaF_3/IBS	LaF_3/PVD1	LaF_3/PVD2
Substrate temperature (°C)	<60	300	300	<60	300	350
Coating stress (MPa)	−910	+385	+300	−1180	+250	+190

[a]Deposition temperature and stress in the MgF_2 and LaF_3 single layers deposited upon special silicon substrates for stress measurements. Compressive stress is indicated by −; tensile stress, by +.

Table 3. Total Backscattering and Surface Roughness[a]

		Process								
		IBS SR and TBS			PVD1 SR and TBS			PVD2 SR and TBS		
			TBS (ppm)			TBS (ppm)			TBS (ppm)	
Substrate	Substrate	SR (nm)	193	633	SR (nm)	193	633	SR (nm)	193	633
Superpolished CaF_2	MgF_2	1.17	470	85.0	1.89	245	12.6	2.12	463	20.0
Superpolished fused silica	MgF_2	1.11	600	1.9	1.51	569	5.7	2.09	940	16.7
Silicon	MgF_2	1.12		5.4	1.17	295	37.6	2.35	795	64.7
Superpolished CaF_2	LaF_3	0.63	290	32.9	2.78	290	8.0	3.30	740	49.0
Superpolished fused silica	LaF_3	0.71	900	116.2	3.13	660	12.1	3.83	810	10.1
Silicon	LaF_3	0.68	440	43.6	3.07	320	4.9			

[a]TBS and surface roughness (SR) of MgF_2 and LaF_3 single layers upon various substrates at wavelengths 193 and 633 nm. The total scatter measurements were evaluated from line scans of the sample surface according to Annex C of standard ISO/DIS 13696.[16] The surface roughness data in column 3 were determined by calculation from surface profiles recorded with an AFM in an area of 10 μm $\times$ 10 μm.

scattering (TS) values of two perpendicular line scans over the sample surface. These scans revealed fairly homogeneous scatter losses across the entire measured sample areas. For each process type in the table, the surface roughness values are also added that were calculated from the AFM topography of a test area with dimensions 10 μm $\times$ 10 μm. For the MgF_2 single layers the lowest scatter losses were achieved with the *e*-beam deposition process on all substrate types investigated. For the boat evaporation process and for IBS, similar scatter values can be observed for CaF_2 substrates. However, a different tendency is observed for the MgF_2 coatings upon fused silica: MgF_2 PVD2 coatings upon superpolished fused-silica substrates exhibited the highest total backward scattering in this experiment. For the MgF_2 PVD coatings, only a slight correlation between the roughness values and the scatter losses can be found: The average surface roughness of MgF_2 PVD coatings, which showed the highest scatter losses in this experiment, clearly exceeds the average roughness values for the competing processes. The relatively high scatter values of the IBS coatings relative to their outstanding low surface roughness values may be based on degradation effects of the substrate during the initial stages of reactive deposition. For example, a chemical reaction of the substrate surface with the reactive fluorine may result in subsurface defects that enhance the optical scattering of the substrate surface without significantly increasing the surface roughness. Considering the various substrate classes, no clear tendency in the total scatter behavior is apparent.

The measured surface roughness of LaF_3 coatings produced by the reactive IBS process was extremely low compared with those of the other coatings in the experiment. Even the though lowest values, in the range 0.6–0.7 nm, were achieved for all substrate types with superpolishing, TBS values at 633 nm were located on a higher level than for the competing coating processes. However, at 193 nm small scatter values that were comparable to the results of the LaF_3 PVD1 were observed for IBS coatings upon CaF_2 substrates.

Established theoretical models based on vector scatter theories and earlier experimental work indicate that no simple relation between roughness and light scattering can be expected for thin-film coatings.[21] In particular, the influence of the interface between the layer and the substrate as well as interface cross-correlation properties, which lead to interference effects of scattered light, can be significant. In studies of one type of single-layer coating, those properties were not accessible. Future detailed investigations will be necessary for proper interpretation of light-scattering properties in terms of interface roughness effects.

In Fig. 3, surface topographies of the MgF_2 and LaF_3 single layers for the coating processes employed within the network are displayed. The contrast of the AFM micrographs, which permits an estimation of the height of the surface profiles, implies a clear ranking of the deposition processes in terms of their surface roughness. For both materials, the most pronounced contrast, which indicates the highest surface roughness, was observed for the PVD2 coatings. The structural features fade for the PVD1 and IBS coatings.

At substrate temperatures near 300 °C, MgF_2 condensed in a columnar structure with an average grain size of approximately 15 nm for a layer thickness of 200 nm.[22] The topography of the MgF_2 PVD2 coating reflects this structure, which is typical for MgF_2 coatings deposited by thermal evaporation: The granular structure of the surface topography can be interpreted as end domes of the columns, which have grown starting in an amorphous MgF_2 zone at the substrate to the surface of the layer. For the MgF_2 PVD1 and MgF_2 PVD2 coatings the average diameter of the columns was determined to range from 20 to 30 nm at the layer surface. The structure of the MgF_2 IBS coatings exhibited granular dimensions in the same regime near 25 nm.

In former studies,[22] typical grain sizes of PVD LaF_3

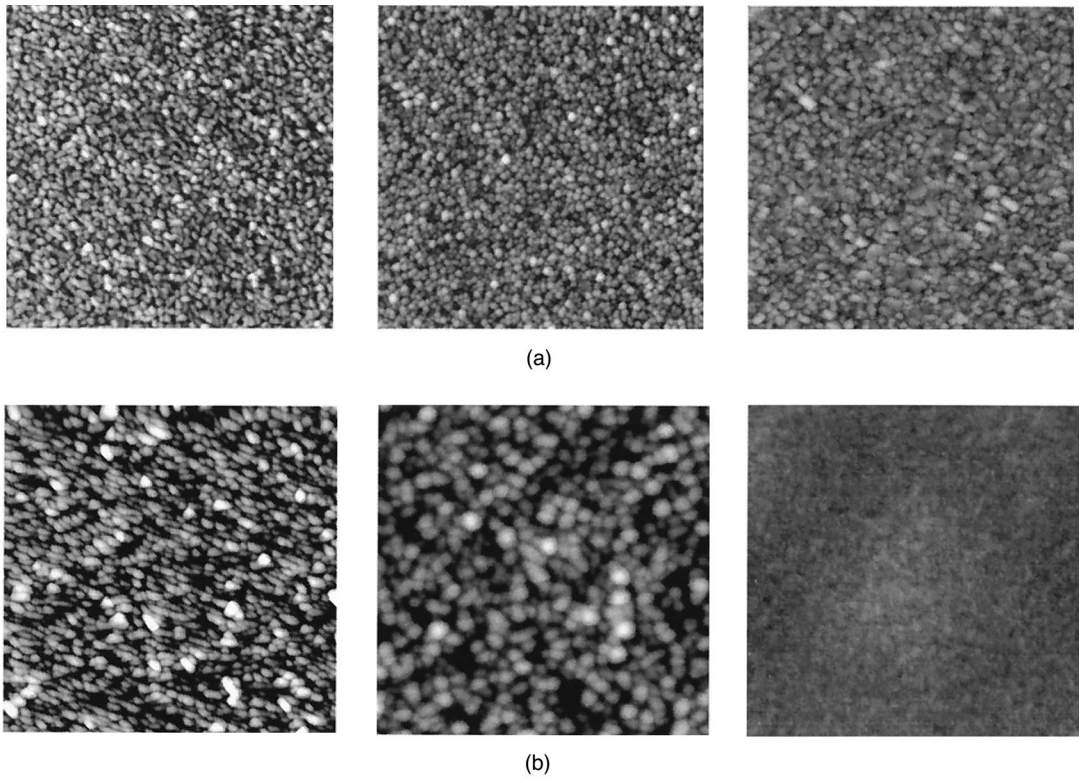

Fig. 3. (a) AFM pictures of selected 1 μm × 1 μm areas of MgF_2 films deposited upon superpolished CaF_2 substrates by three deposition processes: left, PVD2; center, PVD1; right, IBS. The gray scale for the surface profile has a dynamic range from 0 nm (dark) to 20 nm (light). (b) As for (a) but for LaF_3 films. The topography of LaF_3 deposited by PVD1 upon a fused-silica sample is shown.

single layers were determined to approximately 16 nm for a geometric thickness of 180 nm. Also, PVD-deposited layers of LaF_3 exhibit properties similar to those of MgF_2 layers: Near the substrate surface, an amorphous growth zone with randomly oriented isometric crystallites was generally observed. After a polycrystalline phase this structure was transformed into the typical columnar texture with grain sizes, which increased for higher substrate temperatures and increasing layer thicknesses. The AFM micrographs for the PVD LaF_3 single layers suggest slightly larger grains than for the MgF_2 coatings, which were also verified by the higher TBS values of the LaF_3 PVD coatings. In contrast, the surface of the LaF_3 IBS coating can be considered smooth, with only few features.

D. Stoichiometry

In Table 4 the average magnesium and fluorine contents of the MgF_2 and the LaF_3 films are summarized for selected deposition processes. Within the error margins of the XPS analysis employed, good and uniform stoichiometry can be concluded for the MgF_2 layers from the selected deposition processes. The measured ratio of the lanthanum-to-fluorine contents indicates an extremely unbalanced stoichiometry of the LaF_3 single layers, which is in contradiction to the measured optical quality of the coatings. The observed high deficiency of fluorine in the LaF_3 layers can be considered an artifact of the XPS technique: We suspect that argon-ion etching, which was employed for this depth-resolved analysis, leads to preferential sputtering of fluorine atoms from the layer structure. This effect was not observed for MgF_2 coatings because the bonding strength of the fluorine atoms to magnesium is higher than to lanthanum. The spectra of the LaF_3 single layers deposited by IBS affirm the existence of only a small absorptance,

Table 4. Magnesium and Fluorine Content[a]

	Material/Process				
Contents	MgF_2/IBS	MgF_2/PVD1	MgF_2/PVD2	LaF_3/IBS	LaF_3/PVD2
Fluorine (%)	66.9	67.1	67.1	54.2	56.1
Magnesium or fluorine (%)	33.1 Mg	32.9 Mg	32.9 Mg	38.7 La	37.6 La
Ratio	2.02 F/Mg	2.04 F/Mg	2.04 F/Mg	1.39 F/La	1.49 F/La

[a]Average magnesium and fluorine content (XPS measurements) of the MgF_2 and LaF_3 single layers deposited upon Si substrates.

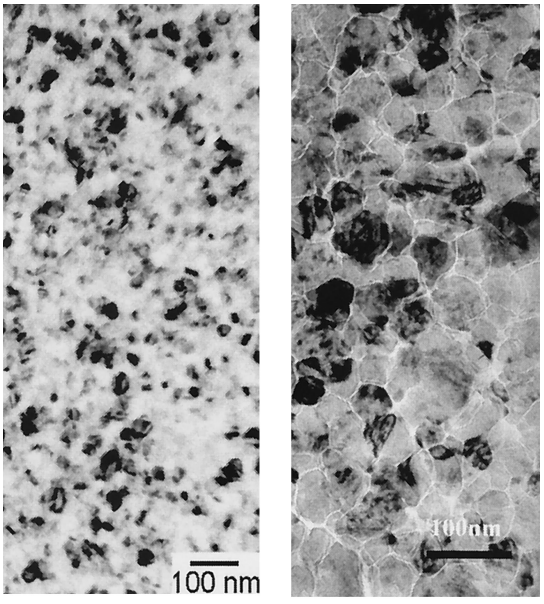

Fig. 4. Transmission electron micrograph of left, a MgF_2 film and right, a LaF_3 film coated by reactive IBS upon silicon substrates (transmission electron micrograph plane view).

which is induced mainly by the residual oxygen contamination in the layers. An oxygen content in total of less than 2% for the MgF_2 layers and of as much as 4% for the LaF_3 films was detected in the coatings produced by the reactive IBS process. In these coatings a low level of carbon was also found.

E. Electron Microscopy

The structural surface properties of the single layers were also investigated by plain-view transmission electron microscopy within the joint experiment. In Fig. 4 plane-view micrographs of MgF_2 IBS and LaF_3 IBS films upon silicon substrates are compared. The grains of the MgF_2 IBS coating [Fig. 4(a)] are randomly oriented, and a medium grain size of approximately 25 nm can be deduced from a statistical evaluation of the micrograph. The same average grain size and homogeneity of grain size distribution were observed for the MgF_2 PVD1 coating. However, the MgF_2 PVD2 layer exhibited a significantly larger medium grain size of 35 nm and poor grain size homogeneity. To gain further insight into the structural properties of MgF_2 layers we performed XRD analysis for selected coating samples upon CaF_2 substrates. The XRD studies revealed a well-defined polycrystalline structure with no apparent differences in the peak intensities and FWHM values of the lines (see Fig. 5). A tetragonal phase ($P4_2/mnm$), which is identical to the rutile structure of bulk MgF_2, can be concluded for all MgF_2 layers. Correspondingly, the average lattice constants deduced from the XRD measurements are in good agreement with the constants of the crystalline material [a(bulk) = 4.625, c(bulk) = 3.052]. An anomalous small peak close to the (110) line and slightly

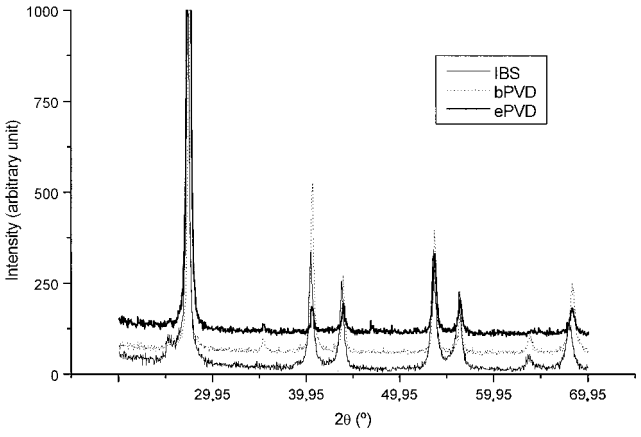

Fig. 5. X-ray diffraction analysis for MgF_2 films upon superpolished CaF_2 substrates (b, boat evaporation; e, e-beam evaporation).

higher lattice constants were observed for the IBS coating.

In the case of the LaF_3 IBS-single layer [Fig. 4(b)], a special structure with an inhomogeneous grain size distribution was found. The grain size varied from 30 to 90 nm; also, very large grains, with dimensions greater than 200 nm, were often observed. The expected hexagonal phase $P3c1$ of bulk LaF_3 could be confirmed in the present study.

To clarify this special topography of the LaF_3 IBS-layers, we performed further electron microscopic investigations on the basis of cross-section techniques [Fig. (6)]. Cross sections of the MgF_2 layers verified tendencies for the structural properties already found in the preceding studies. For example, Fig. 6(a) shows a cross section of a MgF_2 PVD2 coating, which clearly reveals the expected columnar growth of thermally evaporated fluoride films. Besides the coating, which is located at the upper section of the picture, the silicon substrate and a thin oxide layer can be distinguished. The underlying oxide layer can be identified as the native SiO_2 film that is formed upon silicon under normal atmospheric conditions. In this microscopic study the coating thickness was determined to a value of 205 nm, which is located within the thickness values from 201.6 to 208.1 nm calculated on the basis of the dispersion modeling. In the micrograph, the initial growth zone of the layer, which has an amorphous crystalline phase, can be clearly resolved. The columnar growth region following the initial zone is dominated by structural features with a conical shape, which exhibit a size increase toward the surface of the layer. Some of these columns can be traced back to the substrate surface and may reach a diameter of as much as 50 nm at the layer surface. In contrast, cross sections of the MgF_2 IBS coating revealed a regular rectangular shape of the columns in the microstructure with an average column width in the range 20–25 nm. For LaF_3 IBS single layers an analogous structure can be observed [Fig. 6(b)]: Relative to the MgF_2 IBS coating, the LaF_3 layers exhibited a variety of imperfections and crystallites of

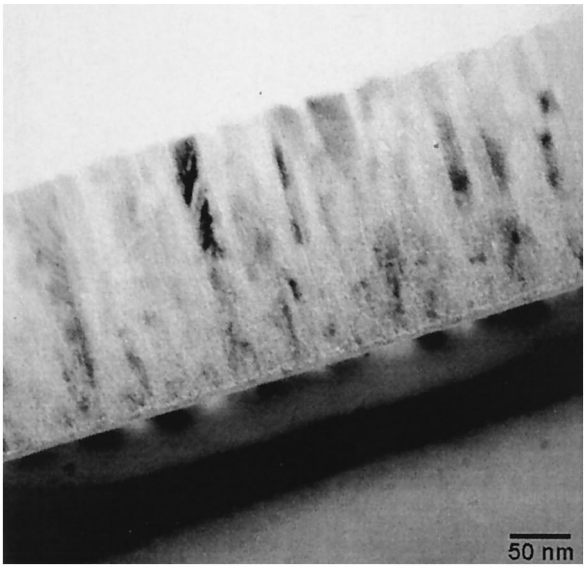

(a)

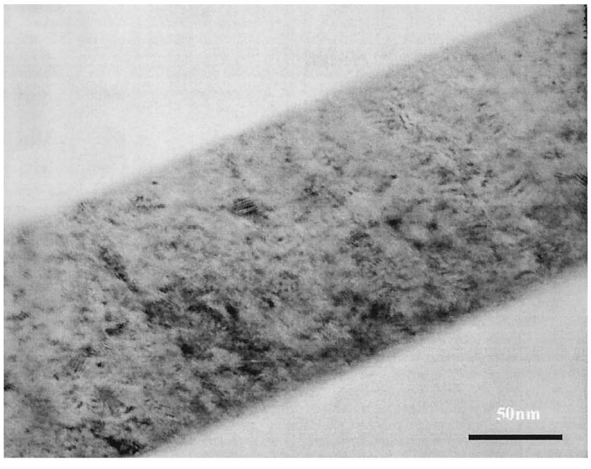

(b)

Fig. 6. Cross-section micrographs of (a) a MgF_2 PVD2-film coated by boat evaporation upon a silicon substrate and of (b) a LaF_3 layer deposited upon a quartz substrate by IBS.

various sizes. As expected from previous studies with plain-view microscopy, the heterogeneous grain size distribution and also randomly distributed large grains can be identified in the cross section. In contrast to the other single layer considered in this study, the texture of the layer is dominated by globular grains.

The difference in the microstructures of fluoride coatings deposited by PVD and by IBS can be interpreted on the basis of the different condensation conditions of these processes. In PVD, the kinetic energy of the admolecules has a Boltzmann distribution with a mean value near 0.1–0.3 eV. Thus the growth of the PVD coatings is mainly a condensation process, with low mobility of the admolecules on the layer surface and shadowing effects by particles already built in the layer. Compared with this growth mechanism, which is strongly dependent on the layer thickness, the sputter process employed for MgF_2 produced particles with average kinetic energies in the range 3–4 eV. Therefore the IBS process is dominated by high-energy condensation with enhanced particle mobility, and, after the first few molecular layers were settled upon the substrate surface, the growth conditions of the IBS coating were nearly constant, with no significant influence from the former development. These conditions resulted in the uniform homogeneous layer structure observed in this study for the MgF_2 IBS layers.

4. Conclusion

A ranking of the selected deposition processes can be established on the basis of the available experimental results for MgF_2 and LaF_3 coatings. Layers deposited by ion-beam sputtering exhibit a refractive index near the bulk value of MgF_2; they have lowest surface roughness of the processes studied; and their microstructure is homogeneous, consisting of regular rectangular columns. MgF_2 IBS coatings suffer from compressive stress, which is attributed to the high energetic growth conditions of these layers. Even though the total backscatter values of LaF_3 IBS films and surface roughness values are lower than the corresponding values of MgF_2 IBS coatings, their microstructural properties are inferior.

The PVD processes investigated in the present study resulted in MgF_2 coatings with higher indices of refraction and a microstructure that contains V-shaped columns and grain sizes of as much as 35 nm. In contrast, the total backward scatter losses of the conventionally deposited films can be less by a factor of 2 than for IBS films, indicating contributions from the volume and the film–substrate interface to the optical scatter behavior of the IBS coatings. The residual stress of the MgF_2 PVD coatings is dominated by the difference in the thermal expansion coefficients of the substrate and the film. For LaF_3 PVD single layers, tendencies similar to those for the MgF_2 PVD coatings were observed.

The present study can be considered a substantial basis for the optimization of optical coating systems for the DUV VUV spectral range. With respect to optical scattering and stability, the best results are expected for layer systems produced by IBS. The highest damage thresholds may be predicted for the PVD processes, which result in coatings with balanced stoichiometry.

The authors gratefully acknowledge the support of the European Commission (TMR-network UV-coatings, contract ERBFMRX-CT97-0101). Also, the authors acknowledge the contributions of Marc Neufert to the deposition of the layers.

References and Notes

1. A. Duparré and N. Kaiser: "Scatter investigation of UV-films: facing the trend towards shorter wavelengths," in *Optical Interference Coatings*" Vol. 9 of 1999 OSA Technical Digest Series (Optical Society of America, Washington, D.C., 1998), pp. 346–347.

2. Papers presented at the International UV Laser Symposium (Lambda Physik), Fort Lauderdale, Fla. November 1–3, 2000,
3. N. T. Sullivan, *Metrology, Inspection, and Process Control for Microlithography XIV*, Proc. SPIE **3998** (2000).
4. J. Ullmann, M. Mertin, C. Zeiss, H. Laut, H. Bernitzki, K. Mann, D. Ristau, W. Arens, R. Thielsch, and N. Kaiser, "Coated optics for DUV—excimer laser applications," in Laser Induced Damage in Optical Materials, G. J. Exarhos, A. H. Guenther, M. R. Kozlowski, K. L. Lewis, and M. J. Soileau, eds., Proc. SPIE **3902,** 514–527 (2000).
5. J. Kolbe, H. Müller, H. Schink, H. Welling, and J. Ebert, "Laser induced damage thresholds at 193 nm and correlations to optical constants and process parameters," in *Laser Induced Damage in Optical Materials*, eds. H. E. Bennett, L. L. Chase, A. H. Guenther, B. E. Newnam, and M. J. Soileau, NIST Spec. Publ. **801**, 404–416 (1989).
6. J. Kolbe, H. Kessler, T. Hofmann, F. Meyer, H. Schink, and D. Ristau, "Optical properties and damage thresholds of dielectric UV/VUV-coatings deposited by conventional evaporation, IAD and IBS," in *Laser Induced Damage in Optical Materials*, H. E. Bennett, L. L. Chase, A. H. Guenther, B. E. Newnam, and M. J. Soileau, eds., Proc. SPIE **1624,** 221–235 (1991).
7. N. Kaiser, B. Anton, K. R. Mann, E. Eva, R. Henking, and D. Ristau, "Laser conditioning of LaF_3/MgF_2-dielectric coatings for excimer lasers," in *Laser-Induced Damage in Optical Materials*: H. E. Bennett, A. H. Guenther, M. R. Kozlowski, 1994; B. E. Newnam, and M. J. Soileau, eds., Proc. SPIE **2428,** 400–409 (1994).
8. For further information see the homepage of the Training and Mobility of Researchers (TMR) network: http://www.lzh.de/tmr/.
9. E. Quesnel, J. Dijon, L. Dumas, P. Garrec, C. Pellé, L. Poupinet, and B. Rolland, "The latest developments in sputtered fluoride films," in *Optical Interference Coatings*, Vol. 9 of 1998 OSA Technical Digest Series (Optical Society of America, Washington, D.C., 1998), pp. 47–49.
10. H. Schink, J. Kolbe, F. Zimmermann, D. Ristau, and H. Welling, "Reactive ion-beam-sputtering of fluoride coatings for the UV/VUV range, in *Laser-Induced Damage in Optical Materials*, H. E. Bennett, L. L. Chase, A. H. Guenther, B. E. Newnam, and M. J. Soileau, eds., Proc. SPIE **1441,** 327–338 (1990).
11. A. Tikhonravov and M. Trubetskov, OptiLayer OptiRE thin-film software, Version 1999, http://www.jcmueller.de/prof_tikhonravov.html.
12. S. Bosch, N. Leinfellner, E. Quesnel, A. Duparré, J. Ferré-Borrull, S. Günster, and D. Ristau, "New procedure for the optical characterization of high-quality thin films," in *Optical Metrology Roadmap for the Semiconductor, Optical, and Data Storage Industries*, G. A. Al-Jumaily, A. Duparré, and B. Singh, eds., Proc. SPIE **4099,** 124–130 (2000).
13. S. Günster, D. Ristau, S. Bosch, "Spectrophotometric determination of absorption in the DUV/VUV spectral range for MgF2 and LaF3 thin films," in *Optical Metrology Roadmap for the Semiconductor, Optical, and Data Storage Industries*, G. A. Al-Jumaily, A. Duparré, and B. Singh, eds., Proc. SPIE **4099,** 299–310 (2000).
14. E. Quesnel, B. Rolland, V. Muffato, D. Labroche and J. Y. Robic, "The ion beam sputtering: a good way to improve the mechanical properties of fluoride coatings," in *Proceedings of the Fortieth Annual SVC Technical Conference* (Society of Vacuum Coaters, Albuquerque, 1997) pp. 293–298.
15. A. Duparré and S. Gliech, "Quality assessment from supersmooth to rough surfaces by multiple-wavelength light scattering measurement, in *Scattering and Surface Roughness*, Z. Gu and A. A. Maradudin, eds. Proc. SPIE **3141,** 57–64 (1997).
16. International Organization for Standardization, "Test method for radiation scattered by optical components," standard ISO/FDIS 13696 (International Organization for Standardization, Geneva, 2000).
17. C. Ruppe and A. Duparré, "Roughness analysis of optical films and substrates by atomic force microscopy," Thin Solid Films **288,** 8–13 (1996).
18. S. Bosch, N. Leinfellner, E. Quesnel, A. Duparré, J. Ferré-Borull, S. Günster, and D. Ristau, "Optical characterization of materials deposited by different processes: the LaF3 in the UV–visible region," M. L. Fulton, in *Optical and Infrared Thin Films*, M. L. Fulton, ed., Proc. SPIE **4094,** 15–22 (2000).
19. E. D. Palik ed. *Handbook of Optical Constants of Solids II*, (Academic, San Diego, Calif., 1991).
20. J. Kolbe and H. Schink, "Optical losses of dielectric VUV-mirrors deposited by conventional evaporation, IAD and IBS," *Thin Films for Optical Systems*, K. H. Guenther, eds., Proc. SPIE **1782,** 435–446 (1992).
21. A. Duparré, "Light scattering of thin dielectric films" in *Thin Films for Optical Coatings*, R. Hummel and K. Guenther, eds. (CRC Press, Boca Raton, Fla., 1995), pp. 273–303.
22. U. Kaiser, "Strukturbedingter Verunreinigungseinbau in dünnen optischen Fluoridschichten," Ph.D. dissertation (Humboldt University, Berlin, 1993) and references therein.